Dalton Transactions

Accepted Manuscript

ROYAL SOCIETY OF CHEMISTRY

www.rsc.org/dalton

Journal Name

ARTICLE

Synthesis and cation distribution in the new bismuth oxyhalides with the Sillén – Aurivillius intergrowth structures

Received 00th January 20xx,

Accepted 00th January 20xx

DOI: 10.1039/x0xx00000x

www.rsc.org/

Dmitri O. Charkin,[a,*] Victor S. Akinfiev[b], Anastasia M. Alekseeva[a], Maria Batuk[c], Artem M. Abakumov[a,c] and Sergey M. Kazakov[a]

About 20 new compounds with the Sillén-Aurivillius intergrowth structure, $Me^1Me^2Bi_3Nb_2O_{11}X$ (Me^1 = Pb, Sr, Ba; Me^2 = Ca, Sr, Ba; X = Cl, Br, I) have been prepared. They are built of stacking of the $[ANb_2O_7]$ perovskite blocks, fluorite-type $[M_2O_2]$ blocks and halogen sheets. The cation distribution between the fluorite and perovskite layers has been studied for $Ba_2Bi_3Nb_2O_{11}I$, $Ca_{1.25}Sr_{0.75}Bi_3Nb_2O_{11}Cl$, $BaCaBi_3Nb_2O_{11}Br$ and $Sr_2Bi_3Nb_2O_{11}Cl$. The smaller Me cations tend to reside in the perovskite block while the larger ones are situated in the fluorite-type block. The distribution of the elements was confirmed for $BaCaBi_3Nb_2O_{11}Br$ using energy dispersive X-ray analysis combined with scanning transmission electron microscopy (STEM-EDX). Electron diffraction study for this compound reveals a local symmetry lowering caused by weakly correlated rotation of NbO_6 octahedra. Based on our findings, we suggest a new stability criterion for mixed-layer structures, which is that net charges of two any consecutive layers do not compensate each other and only the whole layer sequence is electroneutral.

Introduction

The Aurivillius family of layered perovskites, which mainly includes complex bismuth–containing oxides, is famous for its prominent ferroelectric [1,2] and ion conducting [3] properties. Aurivillius phases are constructed of fluorite-related slabs $[Bi_2O_2]^{2+}$ interleaved with the $[A_{n-1}B_nO_{3n+1}]^{2-}$ perovskite slabs of different width (reflected by the index n in their common notation, $\boldsymbol{A}_n$ [4]). Depending on the composition, the Curie points of these materials vary from below room-temperature to ~920°C [5]. However, exhaustive studies of the several past decades seem to have approached the structural and chemical boundaries of this prospective class. In fact, the composition of the perovskite layer is restricted by predominant filling of the B position by d^0-cations with the radius of 0.60 – 0.64Å, i.e. Ti^{4+}, Nb^{5+}, Ta^{5+}, W^{6+}, and sometimes Mo^{6+}, partial substitution by other cations like Fe^{3+} or Ga^{3+} is possible, as a rule, below $^1/_4$ – $^1/_3$, and cations with charge below +3 seem to be "not admitted". From the structural point of view, the maximum "thickness" of the perovskite layer (n) does not probably exceed 6 beyond which the structure becomes disordered [6] or, more probably, converts into different Aurivillius-unrelated arrangements [7]. Further expansion of the Aurivillius-related family is confined to more complex intergrowth or mixed-layer structures (i.e. containing three or more different layers within one unit cell) of which two are hitherto known. In the "homogeneous" series, $\boldsymbol{A}_n\boldsymbol{A}_{n+1}$ (where the $[Bi_2O_2]$ slabs interleave with perovskite blocks of different width), the "thickness" of the perovskite layer is restricted to $n \leq 3$; and the restrictions on chemical composition of the layers seem to be even more severe [8–10].

[a] Department of Chemistry, Moscow State University, 119991, Moscow, Russia.
[b] Department of Materials Sciences, Moscow State University, 119991, Moscow, Russia.
[c] Electron Microscopy for Materials Science (EMAT), University of Antwerp, B-2020, Antwerp, Belgium.
* Corresponding author. Email: charkin@inorg.chem.msu.ru
Electronic Supplementary Information (ESI) available: atomic parameters and selected bond distances for compounds **1** - **4**. See DOI: 10.1039/x0xx00000x

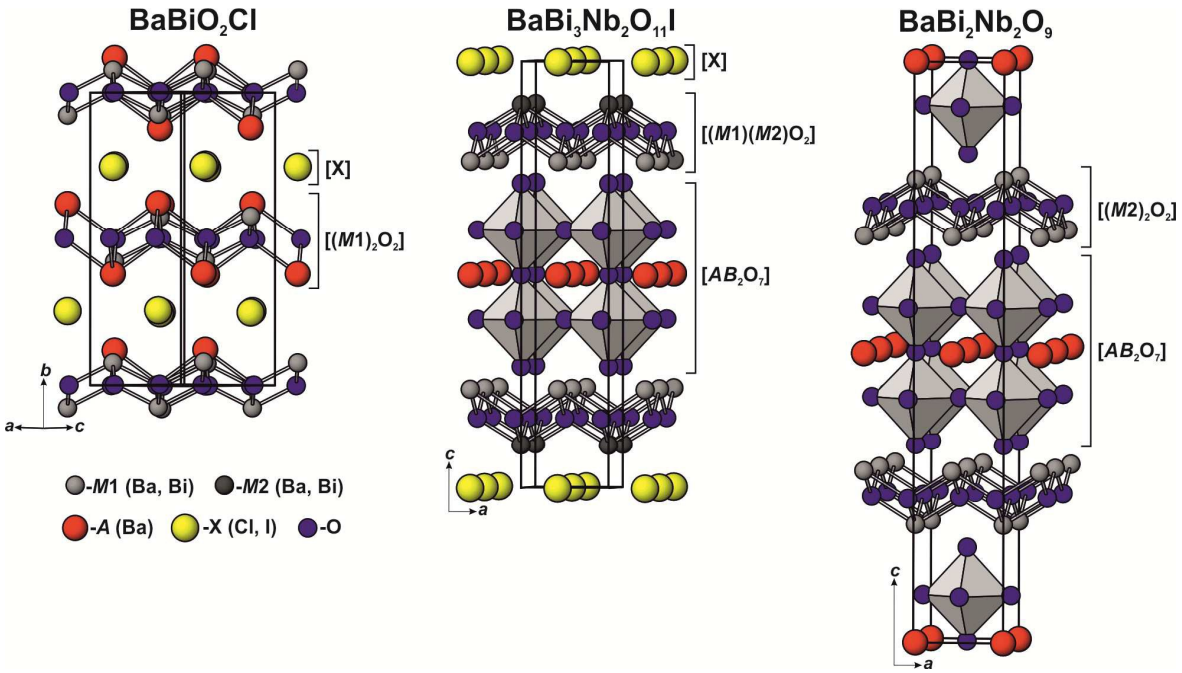

Fig. 1. Crystal structures of (left) Me^1BiO_2X (the orthorhombic structure for Me^1 = Ba); (right) $Me^2Bi_2Nb_2O_9$ type (the tetragonal structure for Me^2 = Ba); (middle) the resulting $Bi_3Me^1Me^2Nb_2O_{11}X$ mixed-layer structure. For the description of *A*, *M*1 and *M*2 positions, see text.

The other opportunity is construction of "heterogeneous" or mixed-layer structures involving structural units from a related Sillén family of bismuth-based compounds where the same $[M_2O_2]$ fluorite slabs are separated by single or double sheets of halide or (less often) chalcogenide anions. These structures can be designated as $\boldsymbol{X}_m$ (*m* = 1 or 2 according to the number of anion sheets).[4] This already vast family, called Bipox (Bismuth perovskite oxyhalides),[11–20] comprise structures where the fluorite layers are separated alternatively by perovskite and halide layers as shown in Fig. 1. These structures are denoted as $\boldsymbol{A}_n\boldsymbol{X}_m$;[4,13–15] as yet only *m* = 1 and $n \leq 4$ members have been reported. Such modification of the Aurivillius structure has significantly expanded the range of cations contributing to these intergrowths both at the sites of fluorite and perovskite slabs. The Bipox compounds commonly retain the ferroelectric properties of Aurivillius archetypes [13–15] though their performances are generally worse.

The complication of both the structure and composition sets the question of cation distribution which is of particular importance since it affects the attempted properties. The most common, yet incompletely studied, is the distribution of Bi^{3+} and some divalent cations between the perovskite $[A_{n-1}B_nO_{3n+1}]$ and the fluorite $[M_2O_2]$ layers. This issue is relevant for the $n \geq 2$ structures; for instance, in $Bi_2MeNb_2O_9$ and $Bi_2MeTa_2O_9$ (Me = Ca, Sr, Ba) a part of alkaline-earth cations filling the *A* perovskite position is exchanged with Bi^{3+} from the fluorite layers, and the transferred amount is roughly proportional to the size of the alkaline-earth cation.[9,21]

In the mixed-layer Bipox structures, the cationic sites in the $[M_2O_2]$ fluorite layers split into two positions, one facing the perovskite layers as in the Aurivillius structures (we denote it *M*1), and the other facing halide layers akin to the Sillén structures (which we denote *M*2, see Fig. 1). Therefore, the cation distribution in these structures is expected to be even more complex. In [22], we have found that in the *n* = 2 Bipox compounds $PbBiO_2X{\cdot}BaBi_2Nb_2O_9$ (X = Cl, Br, I) the Ba/Bi distribution in the Aurivillius part of the structure is the same as in the $BaBi_2Nb_2O_9$. Using the bond valence sum approach, we explained why the Ba^{2+} cations occupy only the sites with oxide coordination (*A* and *M*1 in Fig. 1) leaving the site with mixed oxyhalide environment (*M*2 in Fig. 1) to be occupied by Pb^{2+} and Bi^{3+}. Unfortunately, the distribution of the two latter cations remains an open issue due to practical problems in their distinguishing. This problem also appears in the case of isostructural alkaline-earth compounds, e.g. $Sr_2Bi_3Nb_2O_{11}X$ (X = Cl, Br), which were studied recently by Liu *et al.*.[17] From powder neutron diffraction (PND) data, they established tetragonal symmetry for the $Sr_2Bi_3Nb_2O_{11}Br$. However, because of the relative closeness of scattering lengths for Sr and Bi PND is not very sensitive to the Sr/Bi cation ordering compared to powder X-ray diffraction (PXRD) which is, in turn, less precise in handling light atoms, particularly oxygen. Fray *et al*. [9] highlighted that the mode of handling the thermal parameters (e.g. using overall thermal parameter for all cation positions or separate refinements for alkaline earth and Bi cations, etc.) somewhat affects the refined occupancies in $MeBi_2Nb_2O_9$ (Me = Ca, Sr, Ba); therefore, the issue of the exact cation distribution in these compounds remains open.

The goal of our investigation is to analyze how much the chemical composition of both Sillén and Aurivillius parts

affects the formation of the intergrowth Bipox structure, especially to study the efferc of the size of alkaline-earth cations. We have performed systematic studies of the $Me_2Bi_3Nb_2O_{11}X$ family with Me = Ca, Sr, Ba, Pb, and X = Cl, Br, and I (we retain the symbols *A*, *M*, and *B* only for designation of the corresponding crystallographic sites shown on Fig. 1). Mixed compositions $Me^1Me^2Bi_3Nb_2O_{11}X$ were also addressed. In addition, we considered the possibility of forming intergrowth structures with another $\boldsymbol{X}_1$ compound, Bi_2O_2Se,[23] as well as with a structurally related bismuth oxide selenide, BiOCuSe.[24] Ackerman [12] suggested formation of an $\boldsymbol{A}_1\boldsymbol{X}_2$ intergrowth between the Bi_2WO_6 ($\boldsymbol{A}_1$) and PbFCl ($\boldsymbol{X}_2$) structures; thus, several compositions aimed at the yet unknown $\boldsymbol{A}_2\boldsymbol{X}_2$ structure were also included in the study.

Experimental

Synthesis

The synthetic approach was generally the same as used previously [22] and started from Me^1BiO_2X, Bi_2O_2Se or BiOCuSe and $Me^2Bi_2Nb_2O_9$ precursors prepared according to Ref. 9, 23–25. In the case of mixed-cation oxyhalide compositions, the Me^1 was chosen as Pb^{2+} or smaller alkaline-earth cation. The Sillén-type oxyhalide (oxyselenide) and Aurivillius-type oxide were mixed in (1+δ):1 composition (with $\delta \approx 5$ %) considering the higher volatility of Sillén-like components which is most pronounced for the lead-based compounds [22]. The mixtures (total weight 0.8 – 1 g) were thoroughly ground in agate mortars, pressed into pellets (∅ 8 mm) with a steel die applying pressure of 50 - 80 MPa, sealed into silica tubes under vacuum (X = I) or oxygen (30 kPa at ambient temperature for X = Cl and 5 kPa for X = Br; ampoule volume 3 – 5 ml after sealing), and annealed in a programmable furnace. The phase content of the products was checked by PXRD analysis after each annealing step. Formation of target products was detected in the cases listed in Table 1. The optimized synthesis conditions were found to vary significantly with the nature of both Me^1 and Me^2 and are discussed below. Attempts to prepare selected samples from different precursors (e.g. $BaBiO_2X$ + $CaBi_2Nb_2O_9$ or $CaBiO_2X$ + $BaBi_2Nb_2O_9$) led to products exhibiting nearly identical PXRD patterns.

X-ray Powder Diffraction

Phase identification and lattice parameters determination were performed using room-temperature X-ray powder diffraction data collected in air using Bruker D8-Advance diffractometer (Cu$K_{\alpha1}$ radiation, λ = 1.540598 Å, LynxEye PSD, reflection mode). The program package WinXPOW,[26], TOPAS [27] together with data bases ICDD PDF-2 [28] and ICSD [29] were used for the primary data analysis. We note that processing the patterns with different programs (WinXpoW [26] for phase analysis, TOPAS [27] and JANA2006 [30] for structure refinement) lead to slightly differing results (generally within 0.001Å for *a* and 0.01Å for *c* parameters) which actually does not affect the qualitative pattern and general conclusions.

Electron microscopy

Samples for transmission electron microscopy (TEM) study were prepared by grinding the material under ethanol and depositing a few drops of the suspension onto holey copper grid covered with a thin carbon film. Electron diffraction (ED) patterns were recorded for $BaCaBi_3Nb_2O_{11}Br$ on a Tecnai G2 electron microscope operated at 200 kV. High-angle annular dark-field scanning transmission electron microscopy (HAADF-STEM) images and atomic resolution energy dispersive X-ray spectroscopy (STEM-EDX) elemental maps were collected on a probe aberration-corrected microscope FEI Titian 50-80 equipped with a Super-X detector and operated at 300 kV. Ba-*L*, Ca-*K*, Bi-*L*, Nb-*K*, O-*K* and Br-*K* lines were used for the elemental maps.

The microstructure and the elemental composition were investigated for the $BaCaBi_3Nb_2O_{11}Br$ sample using a JEOL JSM6490LV scanning electron microscope (SEM). The results (at. %, obs/calc: Ca 13(2)/12.5; Br 13(2)/12.5; Nb 26(1)/25; Ba 10(2)/12.5; Bi 38(2)/37.5) are fairly consistent with the suggested composition.

Structure refinement

Four representatives were chosen for the structure determination: $Ba_2Bi_3Nb_2O_{11}I$ (**1**) and $Ca_{1.25}Sr_{0.75}Bi_3Nb_2O_{11}Cl$ (**2**) with the largest and the smallest unit cell parameters, respectively, $BaCaBi_3Nb_2O_{11}Br$ (**3**) with the largest difference between scattering factors of Me^1 and Me^2 which permitted to study their distribution with best possible accuracy and $Sr_2Bi_3Nb_2O_{11}Cl$ (**4**) for a re-investigation of the Sr/Bi cation ordering. Rietveld refinements of the crystal structures of **1** and **2** were performed using room-temperature X-ray powder diffraction data obtained with a STOE STADI-P diffractometer (Co$K_{\alpha1}$-radiation, curved Ge monochromator, transmission mode, linear PSD). The sample of **1** contains < 2 % of the BiOI admixture,[31] which was included into the refinement. Three extremely weak alien reflections (relative intensity below 1 %), partially overlapping with the strongest peaks of the major phase, were found in the pattern of **2**; they were not sufficient to unveil the admixture and finally not addressed. The Rietveld refinement has been performed using the JANA2006 program.[30] Chebyshev polynomials of 10–15th degree were used to describe the background curves. The PXRD profiles were fitted with the pseudo-Voight profile function. Preferred orientation correction with respect to the [001] axis according to March & Dollase was applied. Due to the prominent anisotropic strain broadening the uniaxial model (strain axis [001], **1** case) or tensor one (Stephens formalism,[32] **2** case) was applied. Atomic displacement parameters (ADPs) were refined using isotropic approximation (U_{iso}). For **3** and **4**, the data for

the Rietveld refinement were collected on a Bruker D8/Advance diffractometer (Cu$K_{\alpha 1}$ radiation, LynxEye PSD, reflection mode) and processed using the TOPAS package software.[27] Chebyshev polynomials of 12–15th degree were used to fit the background. Fundamental parameter approach was used for the reflection profiles description. Preferred orientation was corrected using a spherical harmonic approach developed in TOPAS. Atomic displacement parameters (ADPs) were refined using isotropic approximation.

The cation distribution of Bi, Me^1, and Me^2 over the *A*, *M*1, and *M*2 positions was studied by the same way as in Refs. 9 and 22 keeping the overall stoichiometry of the compound, full cation site occupancies and structure electroneutrality. Attempts to refine *z* coordinates and ADPs separately for bismuth and its substituents in the *M*1 and *M*2 positions were successful only for **1** and **3** where the substituent cation (Ba^{2+}) has the largest scattering power and the highest size difference from Bi^{3+}.[33] Final Rietveld refinement plots for **1** and **2** are given in Fig. 2. For **4**, only the Sr/Bi distribution was studied in detail. The refinement details are summarized in Table 2. Calculated atomic parameters and selected bond distances are given in the Supplementary material (Tables S1 – S3).

Initial refinements started from the structure of $Pb_2Bi_3Nb_2O_{11}Cl$ [14]. In case of **1**, the refinement led to the abnormally low ADPs for oxygen atoms compared to those of the heavy atoms. It can be a consequence of complex absorption, poorly accounted in simple models (symmetrical transmission, cylindrical, etc.) It should be noted that in contrast to **1** in case of **2** - **4** the refinement of ADPs for O2 atom led to the anomalously high value. The difference Fourier map revealed two maxima (0, ½ ± δ, *z*) in the vicinity of the O2 site. It allowed to propose the split of O2-position 4*i* (0, ½, *z*) to half-occupied 8*s* (0, *x*, *z*) that corresponds to the split modeling disordered rotations of the NbO_6 octahedra akin to structurally related $Pb_5Fe_3TiO_{11}Cl$ perovskite oxyhalide.[34] This resulted in a drop of residuals together with relatively close values of oxygen ADPs.

Results

Synthesis and PXRD characterization

Three new compounds $Ba_2Bi_3Nb_2O_{11}X$ with X = Cl, Br, I were obtained at the lowest temperature of 800°C after 3–4 consecutive 48-hr annealing steps. The PXRD patterns of all compounds included in Table 1 could be indexed in the tetragonal symmetry akin to the known compounds $Pb_2Bi_3Nb_2O_{11}Cl$, $Sr_2Bi_3Nb_2O_{11}X$ and $PbBaBi_3Nb_2O_{11}X$.[14,17,22] For the oxychloride and oxybromide, traces of unreacted $BaBi_2Nb_2O_9$ were detected. Increasing annealing temperature to 850–880 °C resulted in melting and decomposition of the samples. The $Sr_2Bi_3Nb_2O_{11}Cl$ and $Sr_2Bi_3Nb_2O_{11}Br$ compounds were obtained via a more complex annealing scheme: 800 °C/48 hrs, 850 °C /48 hrs and 1050 °C/2 hrs with intermediate

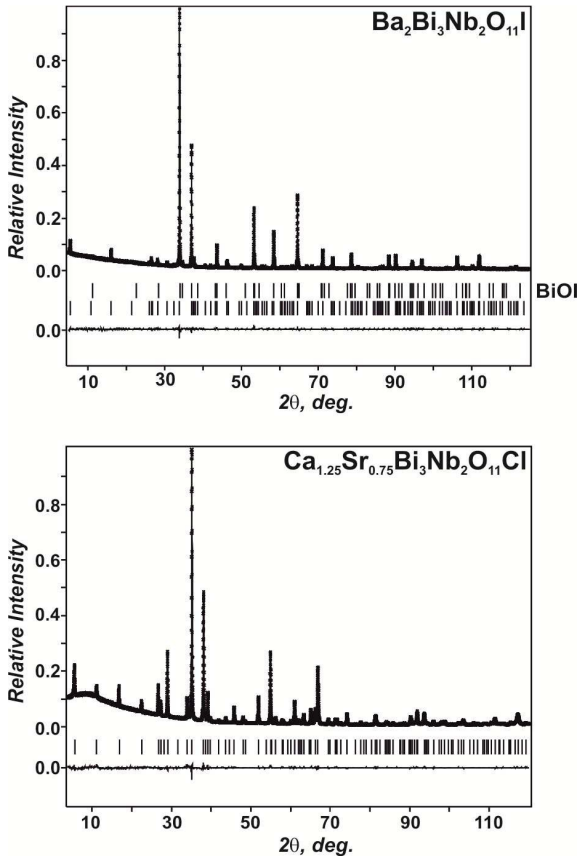

Fig. 2. Experimental, calculated and difference PXRD profiles for **1** and **2** after the Rietveld refinement.

re-grindings. This protocol contains more steps compared to that followed earlier [17] but provides purer samples with better reproducibility. Low-temperature (800 - 850°C) annealing results in formation of only Bi_4NbO_8X (X = Cl, Br [13]) as the major components. The mixed-alkaline-earth oxychlorides and oxybromides were obtained in a similar way with the final annealing step at 950 °C. All oxyiodides listed in Table 1 (other than $Ba_2Bi_3Nb_2O_{11}I$) were synthesized after several annealings at 850 °C. Most of the compounds were prepared single phase or with small amount of admixtures (below 2 % according to the intensity ratio of the strongest lines of target and by-phases). Le Bail fits for three selected compounds are given in Figure S2 (Supplement).

Three compounds $PbSrBi_3Nb_2O_{11}X$ could only be prepared via an "indirect" way of reacting $SrBiO_2X$ with $PbBi_2Nb_2O_9$ at 850 °C, together with small admixtures of $PbBiO_2X$ and $SrBi_2Nb_2O_9$. If the latter were chosen as precursors, no reaction was observed. Although the exact composition of $PbSrBi_3Nb_2O_{11}X$ could not be established, the unit cell parameters of $PbSrBi_3Nb_2O_{11}X$ differ from those of $Sr_2Bi_3Nb_2O_{11}X$ indicating incorporation of Pb^{2+} into the structure ($Pb_2Bi_3Nb_2O_{11}Br$ and $Pb_2Bi_3Nb_2O_{11}I$ probably do not exist [17]). Reactions between $CaBiO_2X$ and $PbBi_2Nb_2O_9$ result in similar PXRD patterns, however, these contain split (00*l*)

reflections and the calculated cell parameters vary significantly with the number of annealing cycles. The composition and structure of the Pb/Ca compounds formed is yet uncertain and they will be reported separately after further studies.

Table 1 Unit cell parameters for the new $Me^1Me^2Bi_3Nb_2O_{11}X$ oxyhalides

Compound	a, Å	c, Å	V, Å^3
$Ba_2Bi_3Nb_2O_{11}Cl$	3.9697(5)	18.747(5)	295.4
$Ba_2Bi_3Nb_2O_{11}Br$	3.9784(6)	18.983(5)	300.4
$Ba_2Bi_3Nb_2O_{11}I$	3.9929(1)	19.2771(5)	307.3
$BaSrBi_3Nb_2O_{11}Cl$	3.9359(6)	18.662(5)	289.1
$BaSrBi_3Nb_2O_{11}Br$	3.9490(4)	18.806(4)	293.3
$BaSrBi_3Nb_2O_{11}I$	3.9599(6)	19.205(5)	301.2
$BaCaBi_3Nb_2O_{11}Cl$	3.9007(1)	18.656(3)	283.9
$BaCaBi_3Nb_2O_{11}Br$	3.9077(1)	18.8708(6)	288.2
$BaCaBi_3Nb_2O_{11}I$	3.9183(9)	19.220(5)	295.1
$Sr_2Bi_3Nb_2O_{11}Cl$	3.9149(1)	18.4767(2)	283.1
$Sr_2Bi_3Nb_2O_{11}Br$	3.9222(1)	18.6618(2)	287.1
$Sr_2Bi_3Nb_2O_{11}I$	3.9397(4)	19.032(4)	295.4
$Sr_{0.75}Ca_{1.25}Bi_3Nb_2O_{11}Cl$	3.8782(1)	18.3889(4)	276.6
$SrCaBi_3Nb_2O_{11}Cl$	3.8806(1)	18.4011(4)	277.1
$SrCaBi_3Nb_2O_{11}Br$	3.8965(5)	18.616(3)	282.6
$SrCaBi_3Nb_2O_{11}I$	3.9142(6)	19.024(6)	291.5
$PbSrBi_3Nb_2O_{11}Cl$	3.9078(4)	18.811(2)	287.3
$(Pb,Sr)_2Bi_3Nb_2O_{11}Br$ [1]	3.9246(5)	18.808(3)	289.7
$(Pb,Sr)_2Bi_3Nb_2O_{11}I$ [1]	3.937(1)	19.096(8)	296.0

[1] The samples contain small amounts of $PbBiO_2X$ and $SrBi_2Nb_2O_9$, the Pb/Sr ratio probably deviates from 1.

No new $\boldsymbol{A_2X_1}$ compound was observed with $Me^1 = Me^2 = Ca$ at 850–1050 °C and in all oxyselenide compositions at 800–850 °C (just below the decomposition points of the oxyselenides). Attempts to prepare $Sr_{1-x}Ca_{1+x}Bi_3Nb_2O_{11}Cl$ solid solution gave a maximum value of $x \approx 0.25$. The PXRD patterns of the samples $MeBi_2Nb_2O_9{\cdot}2BiOX$ aimed at the $\boldsymbol{A_2X_2}$ composition had nothing in common with the calculated patterns of the proposed $\boldsymbol{A_2X_2}$ compounds.

TEM study

TEM analysis was performed for $BaCaBi_3Nb_2O_{11}Br$, in order to check the existence of superstructure and to confirm the cation distribution found from the PXRD studies. Electron diffraction patterns of $BaCaBi_3Nb_2O_{11}Br$ are given in Figure 3. The patterns were indexed in the tetragonal *P*4/*mmm* subcell (subscript "t" is added) with a ≈ 3.9 Å, c ≈ 18.9 Å unit cell parameters. However, lines of weak diffuse intensity can be noticed on the $[110]_t$ and $[310]_t$ ED patterns (indicated with arrows in Figure 3). As commonly observed for layered perovskite oxyhalides, they can be caused by the disordered rotations of the NbO_6 octahedra in the perovskite block (see Section 4.2). Intersection of these diffuse intensity lines with the Ewald sphere causes the extra *h*/2,*k*/2,0, *h*, *k* – odd reflections on the $[001]_t$ pattern.

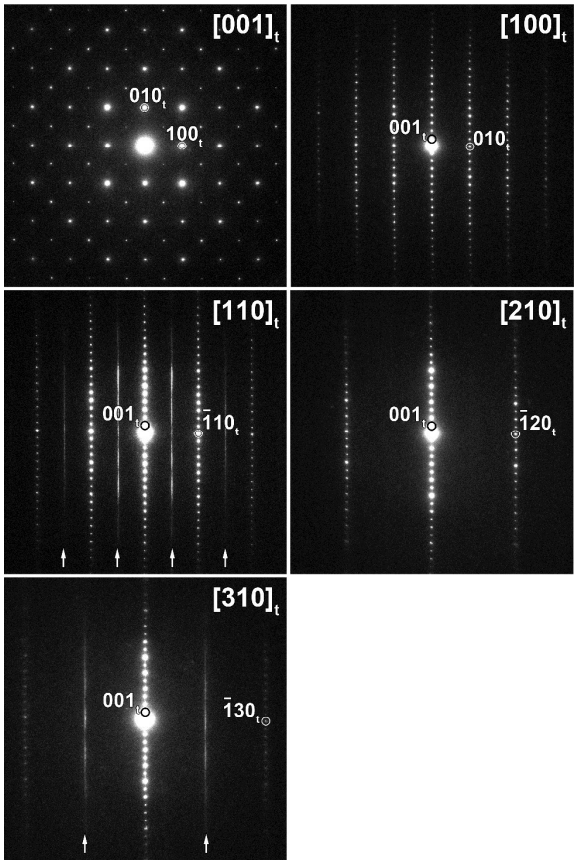

Figure 3. Electron diffraction patterns of $BaCaBi_3Nb_2O_{11}Br$. The lines of diffuse intensity on the $[110]_t$ and $[310]_t$ ED patterns are marked with arrows. Extra *h*/2,*k*/2,0, *h*, *k* – odd reflections on the $[001]_t$ patterns are due to the intersection of these lines with the Ewald sphere.

HAADF-STEM image of $BaCaBi_3Nb_2O_{11}Br$ taken along the most informative $[100]_t$ direction is shown in Figure 4. The unit cell is outlined on the image with the white rectangle (for the interpretation see Fig. 1). The brightness of the dots on the HAADF-STEM image scales approximately as $Z^{1.6\text{-}1.9}$, where Z is an average atomic number of the projected columns. The dark lines on the image correspond to the layers of the *A* cations (Z_{Ca} = 20, indicated with red arrowheads in Figure 4). The *M*2 positions are the brightest and correspond to the Bi positions (Z_{Bi} = 83). The *M*1 positions look slightly darker since they are occupied by the mixture of Bi and Ba cations (Z_{Ba} = 56). The layers of the Br atomic columns are easily distinguishable (Z_{Br} = 35) and they are indicated with the blue arrowheads.

To confirm the elements' distribution in the structure, atomic resolution STEM-EDX mapping was performed (Figure 5). According to the maps and the corresponding intensity profiles (see Supporting Information), the *A* positions are almost fully occupied by the Ca cations, *M*1 – by the ~1:1 mixture of Ba and Bi, and *M*2 – purely by Bi. Therefore, the cation ordering patterns determined from the STEM-EDX closely resemble the results of the Rietveld analysis (see Supplement, Table S2).

Table 2 Data collection and crystallographic parameters for compounds **1** - **4**

Compound	**1**	**2**	**3**	**4**
Phase purity	Target phase 97.9(1) wt.% BiOI [1] 2.1(1) wt.%	Single phase	Single phase	Target phase 97.6(1) wt.% $SrBi_2Nb_2O_9$ [2] 3.4(1) wt.%
Crystal system	Tetragonal			
Space group	*P*4/*mmm*(# 123)			
a, Å	3.99093(1)	3.87820(3)	3.90707(9)	3.9136(1)
c, Å	19.2694(1)	18.3888(2)	18.8687(5)	18.4711(2)
V, Å^3	306.912(2)	276.575(4)	288.04(1)	282.9(1)
Z	1			
Calculated density, g·cm^{-3}	7.522	6.796	7.29	7.04
Radiation	Co$K\alpha_1$ (λ = 1.78892Å)		Cu$K\alpha_1$ (λ = 1.54059Å)	
Absorption coefficient, mm^{-1}	248.29	179.79	138.19	117.56
2θ range, °	4.90–125.09	3.90–119.82	8.0 – 100.0	8.0 – 100.0
Number of points	12020	11620	4372	6120
Number of observed reflections (I> 3σ)	118	121	107	116
Refined profile parameters	18	27	26	28
Refined structural parameters	19	16	20	18
R_I, R_{exp}	0.023, 0.042	0.026, 0.034	0.016, 0.039	0.020, 0.044
R_p, R_{wp}	0.032, 0.043	0.030, 0.041	0.050, 0.074	0.049, 0.065
χ^2	1.05	1.48	1.91	1.48

[1] BiOI: space group *P*4/*nmm* (# 129), *Z* = 2, *a* = 3.999(1) Å, *c* = 9.171(1) Å [ICSD #391354]; R_I = 0.043.

[2] $SrBi_2Nb_2O_9$: space group *A*2$_1$*am* (# 36), *Z* = 4, *a* = 5.513(2) Å, *b* = 5.509(2) Å, *c* = 27.075(4) Å [ICSD #82280], R_I = 0.043.

Results

New compounds and compositions

Successful preparation of over ten new derivatives of $Pb_2Bi_3Nb_2O_{11}Cl$ indicates that in this structure the lead cations can be completely substituted by alkaline-earth cations with the only exception of $Ca_2Bi_3Nb_2O_{11}X$ and probably $PbCaBi_3Nb_2O_{11}X$ compositions. Along with oxychlorides and oxybromides, we succeeded in preparation of numerous oxyiodides which already seem to be rather common in this family [22,35]. The minimal value of the *a* parameter, which probably determines the closest $I^- - I^-$ contacts, is observed in this family for $SrCaBi_3Nb_2O_{11}I$ and equals 3.91Å which is quite close to the minimal value observed among the Sillén-type Bi oxyhalides (3.94Å for $LiBi_3O_4I_2$ [4, 25]). All attempts to prepare analogous oxide chalcogenides have yet failed; the possible reasons will be discussed below. Since the compounds were prepared with the purity of 98% and higher, we suggest that their actual compositions do not strongly deviate from those listed in Table 1.

The data listed in Table 1 indicate that in the $Ba_2Bi_3Nb_2O_{11}X$ – $BaSrBi_3Nb_2O_{11}X$ – $BaCaBi_3Nb_2O_{11}X$ and $Sr_2Bi_3Nb_2O_{11}X$ – $SrCaBi_3Nb_2O_{11}X$ series (when X is not varied), the expected shrinking of the unit cell volume occurs mostly due to decrease of the *a* unit cell parameter, whereas the *c* cell parameter remains almost insensitive to the nature of the alkaline-earth cation. On going from $MeBi_2Nb_2O_9$ (Me = Ca, Sr, Ba) to

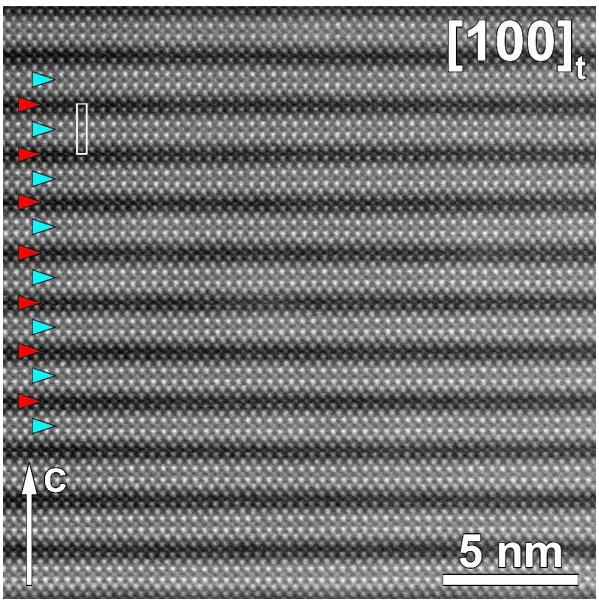

Figure 4. HAADF-STEM image of $BaCaBi_3Nb_2O_{11}Br$. Red arrowheads indicate the layers of the *A* positions (Ca), blue – the Br layers. The unit cell is outlined.

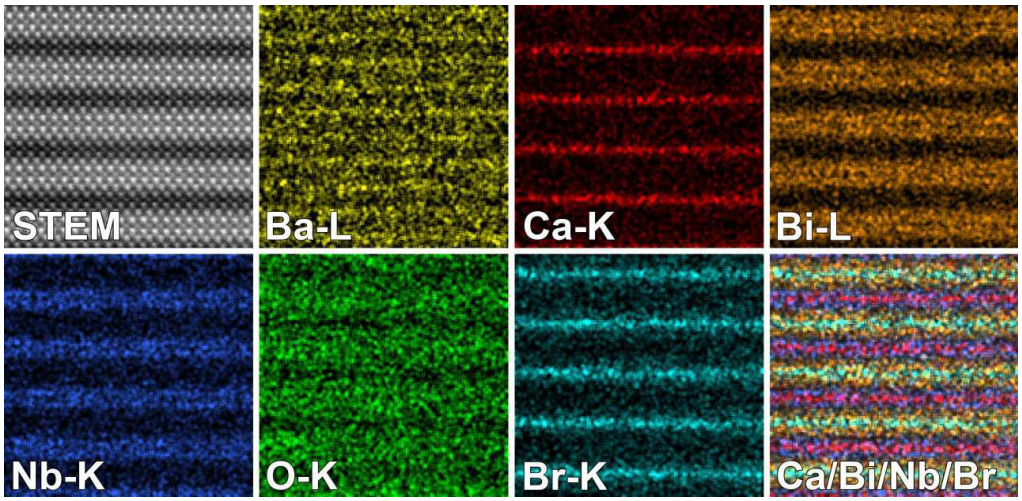

Figure 5. HAADF-STEM image, atomic resolution STEM-EDX elemental maps and a Ca/Bi/Nb/Br mixed map for $BaCaBi_3Nb_2O_{11}Br$.

$BaMeBi_3Nb_2O_{11}X$, the *a* parameter increases by *ca*. 0.034Å for X = Cl, *ca*. 0.045Å for X = Br and *ca*. 0.057Å for X = I. A similar behaviour is observed for the $SrMeBi_3Nb_2O_{11}X$ series (Me = Ca, Sr). Increments were also observed in the cell volumes: *ca*. 3.5Å^3 on going from chlorides to bromides, and *ca*. 7Å^3 on going from bromides to iodides. This is roughly proportional to the difference of the volumes of halide ions calculated from their ionic radii.[33] This does not exactly hold for the compounds $(Pb,Sr)_2Bi_3Nb_2O_{11}X$ which were not obtained single-phase and where the composition is likely to deviate from the Pb:Sr = 1:1 ratio.

Crystal structures

As follows from both TEM data (Fig. 4) and the Rietveld refinements, the crystal structures of the new compounds are similar to those of $Pb_2Bi_3Nb_2O_{11}Cl$ and $PbBaBi_3Nb_2O_{11}X$ [14,22] and can be described as an ordered sequence of fluorite, perovskite and halide layers: $[Bi_{2-x}Me_xO_2]$-[X]-$[Bi_{2-x}Me_xO_2]$-$[Me_{1-y}Bi_yNb_2O_7]$-$[Bi_{2-x}Me_xO_2]$ -... (Fig.1). Though the average symmetry of these compounds is tetragonal, local deviations similar to those typical for Aurivillius phases are likely present. The recent PND studies of $Sr_2Bi_3Nb_2O_{11}X$ revealed no indications of local symmetry lowering, according to close values of thermal parameters of all atoms, particularly those occupying special positions. However, in the case of $Ca_{1.25}Sr_{0.75}Bi_3Nb_2O_{11}Cl$ and $BaCaBi_3Nb_2O_{11}Br$ the deviations from the ideal arrangement do exist; they can be *on average* modeled by rotations of the NbO_6 octahedra around the *c*-axis. The weakly correlated nature of these rotations is indicated by the diffuse intensity lines on the ED patterns. These rotations are present in the structures of $BaCaBi_3Nb_2O_{11}Br$ and $Sr_{0.75}Ca_{1.25}Bi_3Nb_2O_{11}Cl$ where the *A* perovskite position is occupied by the smallest Ca cations and Goldschmidt tolerance factors are the lowest. When the *A* positions are occupied by Sr or Ba, as in $Sr_2Bi_3Nb_2O_{11}Cl$ [17] and $Ba_2Bi_3Nb_2O_{11}I$, the structure is more regular. We note that while these Bipox structures are tetragonal, the corresponding Aurivillius phases $SrBi_2Nb_2O_9$ and probably $BaBi_2Nb_2O_9$ are not.[9] As we had observed earlier for *n* = 1 Bipox compounds,[35] the archetypic centrosymmetric tetragonal structure is easily restored when the initial acentric orthorhombic Aurivillius structure is "diluted" by weakly polarizable halide anions and when the *M*1 positions are filled by relatively large cations with no lone pairs which is indeed the case in the compounds considered in this study. This tendency is likely to be present in the structures of higher homologues with *n* > 2 which are currently under study.

It is worth noting that weakly correlated octahedral rotations are likely to be present in the structure of $Pb_2Bi_3Nb_2O_{11}Cl$, wherein the superstructure suggested from ED patterns was found neither on PND nor on PXRD patterns.[14] The [001] ED patterns of $Pb_2Bi_3Nb_2O_{11}Cl$ [14] and $BaCaBi_3Nb_2O_{11}Br$ (this work) look very similar; unfortunately, the [110] pattern (where the diffuse or ordered intensity can be seen) is not provided for $Pb_2Bi_3Nb_2O_{11}Cl$. The PND refinement of this structure performed in the same study yielded a very high thermal parameter for the O2 atom. It is very likely that the O2 from is also shifted form the ideal 00*z* position in $Pb_2Bi_3Nb_2O_{11}Cl$.

The trends in Me^1/Me^2 cation ordering in the structures of the new $Me^1Me^2Bi_3Nb_2O_{11}X$ compounds can be explained the same way as for the $PbBaBi_3Nb_2O_{11}X$ members of the family.[22] For Ba^{2+}, bond valence sum (BVS) calculations for different cation positions reveal a slight overbonding for *A* and very severe overbonding for *M*2, while for *M*1 the sum can equal 2 at a certain reasonable value of the *z* coordinate. Therefore, Ba^{2+} occupies the *A* site only in the structure of $Ba_2Bi_3Nb_2O_{11}I$ (and, evidently, the other $Ba_2Bi_3Nb_2O_{11}X$ compounds). In $BaCaBi_3Nb_2O_{11}Br$, Ca^{2+} and Ba^{2+} are distributed according to their preferences to the *A* and *M*1 positions, respectively. Similar BVS calculations for Sr^{2+} and Ca^{2+} indicate that the BVS(Sr) can equal 2 both in the oxide and oxyhalide

environment at reasonable bond distances. This means that Sr^{2+} and Ca^{2+} can distribute over both *M*1 and *M*2 sites which is indeed observed in the structures of $Sr_2Bi_3Nb_2O_{11}Cl$ and $Sr_{0.75}Ca_{1.25}Bi_3Nb_2O_{11}Cl$. The BVS calculations also help to explain the absence of barium analogs of the known Ca(Sr) – Bi oxyhalides $MeBi_2O_3X_2$ and $MeBi_3O_4X_3$ where all cations reside in mixed oxide-halide environment [4] unfavorable for Ba^{2+} upon tetragonal symmetry and mixed Me/Bi site occupancies.[22]

Compatibility criteria for the intergrowth structures

We did not succeed in preparing the desired intergrowth structures for the Bi_2O_2Se, BiOCuSe, and BiOX compounds. The possibility of obtaining a certain layered structure is often considered to depend on the overall electroneutrality of the system, chemical (mostly redox), and geometrical (size match for commensurate structures) compatibility (reviewed recently [36,37]). As yet, we restrict our consideration to the structures where the interactions between the layers are of predominantly non-covalent (electrostatic or Van-der-Waals) nature [36,38] and net layer charges (per unit cell) can be considered. In [22,36], we demonstrated that these criteria can indeed be propagated into the realm of mixed-layer structures considering the layered sequences as the intergrowing building blocks. The criterion of geometrical compatibility can be formulated in terms of cell parameter mismatch of the building blocks; in our case $\Delta=2\cdot\left|(a_1-a_2)/(a_1+a_2)\right|$. A survey of the known $\boldsymbol{A}_1\boldsymbol{X}_1$-type compounds and solid solutions [39] suggests that a formation of the intergrowth structure can hardly be expected when Δ exceeds 0.03. However, both Bi_2O_2Se and BiOCuSe satisfy this criterion when considered together with $BaBi_2Nb_2O_9$. Therefore, the criterion of geometric compatibility is not sufficient and another one should be addressed when considering formation of intergrowth structures from simpler and *initially neutral* layer sequences (Aurivillius and Sillén structures for the compounds considered herein). When an intergrowth ***ABAC*** structure is formed from ***AB*** and ***AC*** layer sequences, the composition of the ***A*** layers, common for both structures, should average between ***AB*** and ***AC***. For the structures shown in Fig. 1, the compositions of the common fluorite slabs are $[(Me_{0.5}Bi_{0.5})_2O_2]^+$ and $[Bi_2O_2]^{2+}$. Upon formation of the intergrowth, the mean composition should become $[Bi(Me_{0.5}Bi_{0.5})O_2]^{1.5+}$ which results in the Aurivillius and Sillén parts losing their electroneutrality to yield $\{[Bi_{1.5}Me_{0.5}O_2]^{1.5+}[MeNb_2O_7]^{2-}\}^{0.5-}$ and $\{[Bi_{1.5}Me_{0.5}O_2]^{1.5+}[X]^-\}^{0.5+}$, thus only the complete layer sequence remains neutral. This is inherent for the compounds like Bi_4NbO_8Cl ($\boldsymbol{A}_1\boldsymbol{X}_1$) [11] and $Bi_6Ti_2MO_{14}Cl$ ($\boldsymbol{A}_3\boldsymbol{X}_1$; M = Cr, Fe, Mn).[19] In the case of Bi_2O_2Se (BiOCuSe) and $BaBi_2Nb_2O_9$, the composition of the fluorite layers is virtually the same, and re-distribution of dissimilarly charged cations is not feasible (the small amount of Ba^{2+} present in the fluorite layers in $BaBi_2Nb_2O_9$ [9] is probably not sufficient to stabilize the intergrowth). The same applies to the structure of the recently discovered compound $PbBi_4O_6Cl_2$ [40] which features the $[PbBi_2O_4]^0[Cl]^-[Bi_2O_2]^{2+}[Cl]^-$ layer sequence which is neutral only as the whole. Such redistributions have been observed in the majority of known intergrowth structures among compounds not only of bismuth. For instance, oxide pnictides of rare-earths with the BiOCuSe (LaOAgS) structure can be prepared in single-crystalline forms from alkali chloride melt.[41] However, attempts to apply this procedure to grow structurally related $Ln_3O_{2-x}Cu_4Pn_4$ (Pn = P, As; $x \approx 0.5$) resulted in more complex layered structures of $Ln_5O_{4-x}Cu_4Pn_4Cl_2$,[42] which are intergrowths between $Ln_3O_{2-x}Cu_4Pn_4$ and LnOCl. Therein, the intergrowth is stabilized by redistribution of oxygen vacancies over the fluorite slabs: $[Ln_2O_{1.5}]^{3+}[LnCu_4Pn_4]^{3-} + [Ln_2O_2]^{2+}[Cl_2]^{2-} \rightarrow \{[Ln_2O_{1.75}]^{2.5+}[LnCu_4Pn_4]^{3-}\}^{0.5+}\{[Ln_2O_{1.75}]^{2.5+}[Cl_2]^{2-}\}^{0.5-}$. In the case of $[Ln_2O_2]^{2+}[T^{II}{}_2Pn_2]^{2-}$ (T^{II} = divalent transition metal) and $[Ln_2O_2]^{2+}[Cl_2]^{2-}$, no exchange among fluorite layers is feasible, and anion exchange between Pn^{3-} and Cl^- is hardly possible due to gross differences in bonding character and preferences; therefore, formation of intergrowths is unlikely; they have not been observed indeed. Yet another example is the structure of a recently discovered compound $Pr_4Fe_2O_4Te_{0.88}$ = $[Pr_2O_2]^{2+}[Fe_2As_2]^{2.24-}[Pr_2O_2][Te_{0.88}]^{1.76-}$; the electroneutrality is provided by oxidation state of Fe below +2 which is consistent with the compound being a medium-temperature superconductor.[43]. Therefore, another criterion is added which suggests that a mixed-layer structure is stable against several simpler (bi-layer) structures when only the whole layer sequence is electroneurtal while the net charges of any two successive cationic and anionic layers within it do not compensate each other. As that of geometrical compatibility, this criterion is probabilistic: several interesting exceptions come from structurally related but chemically different oxyhalides of lead where the molar percentage of bismuth is small.[44] New targeted studies are expected to unveil the trends in behavior of these peculiar compounds in more details and to help preparation of new members with tailored structures and properties.

Conclusions

In comparison to the $PbBi_3WO_8Cl$-based solid solutions and $PbBaBi_3Nb_2O_{11}X$, the structures of $Me^1Me^2Bi_3Nb_2O_{11}X$ demonstrate significant cation redistributions compared to their building blocks, Me^1BiO_2X and $Me^2Bi_2Nb_2O_9$. First, there is an almost complete ordering of Me^1 and Me^2 between $[ANb_2O_7]$ and $[M1M2O_2]$ blocks (the smaller cations strongly tend to the former). Second, the Me^1 cation changes, at least partially, its environment from mixed-anion (oxygen + halogen) into pure-oxygen. This kind of *A*/*M*1/*M*2 cation ordering is likely to be characteristic for intergrowth structures based on higher ($n > 2$) homologues of the Aurivillius phases. We also suggest a new compatibility criterion for targeting mixed-layer structures particularly when they are formed via intergrowth of more simple, thus initially neutral layer sequences.

Acknowledgements

The work was supported by the Russian Scientific Foundation under Grant No.14-13-00738. We are also grateful for the unknown referees for helpful comments.

Notes and references

1 C.A.Paz de Araujo, J.D. Chuchiaro, L.D. McMillan, M.C. Scott, J.F. Scott, *Nature (London)* 1995, **374**, 627–629.
2 E.C. Subbarao, *J. Phys. Chem. Solids* 1962, **23**, 665–676.
3 J.C. Boivin and G. Mairesse, *Chem. Mater.* 1998, **10**, 2870–2888.
4 V.A. Dolgikh and L.N. Kholodkovskaya, *Russ. J. Inorg. Chem.* 1992, **37**, 970–985.
5 V.I. Voronkova, E.P. Kharitonova, and O.G. Rudnitskaya, *J. Alloys Compd.* 2009, **487**, 274–279.
6 S. Borg, G. Svensson, and J.O.Bovin, *J. Solid State Chem.* 2002, **167**, 86–96.
7 Ismunandar, Brendan J. Kennedy, Gunawan, Marsongkohadi, *J. Solid State Chem.* 1996, **126**, 135–141.
8 P. Boullay, L. Palatinus, and N. Barrier, *Inorg. Chem.* 2013, **52**, 6127–6135.
9 S.M. Blake, M.J. Falconer, M. McCreedy, and P. Lightfoot, *J. Mater. Chem.* 1997, **7**, 1609–1613.
10 N.C. Hyatt, J.A. Hriljac, and T.P. Comyn, *Mat. Res. Bull.* 2003, **38**, 837–846.
11 B. Aurivillius, *Chem. Scr.* 1984, **23**, 143–156.
12 J.F. Ackerman, *J. Solid State Chem.* 1986, **62**, 92–104.
13 A.M. Kusainova, W. Zhou, J.T.S. Irvine, and P. Lightfoot, *J. Solid State Chem.* 2002, **166**, 148–157.
14 A.M. Kusainova, P. Lightfoot, W. Zhou, S.Yu. Stefanovich, A.V. Mosunov, and V.A. Dolgikh, *Chem. Mater.* 2001, **13**, 4731–4737.
15 A.M. Kusainova, S.Yu. Stefanovich, J.T.S. Irvine, and P. Lightfoot, *J. Mater. Chem.* 2002, **12**, 3413–3418.
16 S. Liu, W. Müller, Y. Liu, M. Avdeev, and C. D. Ling, *Chem. Mater.* 2012, **24**, 3932–3942.
17 S. Liu, P.E.R. Blanchard, M. Avdeev, B.J. Kennedy, and C.D. Ling, *J. Solid State Chem.* 2013, **205**, 165–170.
18 D. Ávila-Brande, Á.R. Landa-Cánovas, and L.C. Otero-Díaz, *Chem. Mater.* 2007, **19**. 323–328.
19 D. Ávila-Brande, L.C. Otero-Díaz, Á.R. Landa-Cánovas, S. Bals, and G. Van Tendeloo, *Eur. J. Inorg. Chem.* **2006**, 1853–1858.
20 D. Ávila-Brande, Á.R. Landa-Cánovas, and L.C. Otero-Díaz, *Acta Cryst.* 2008, **B64**, 438–447.
21 R. Macquart, B.J. Kennedy, and Y. Shimakawa, *J. Solid State Chem.* 2001, **160**, 174–177.
22 D.O. Charkin, D.N. Lebedev, and S.M. Kazakov, *Russ. J. Inorg. Chem.* 2012, **57**, 917–922.
23 P. Schmidt, O. Rademacher, H. Oppermann, and S. Däbritz, *Z. Anorg. Allgem. Chem.* 2000, **626**, 1999–2003.
24 H. Hiramatsu, H. Yanagi, T. Kamiya, K. Ueda, M. Hirano, and H. Hosono, *Chem. Mater.* 2008, **20**, 326–334.
25 D.O. Charkin, P.S. Berdonosov, V.A. Dolgikh, and P. Lightfoot, *J. Solid State Chem.* 2003, **175**, 316–321.
26 STOE WinXPOW, Version 1.2, STOE & Cie GmbH, Darmstadt, Germany, 2000.
27 TOPAS V3, General Profile and Structure Analysis Software for Powder Diffraction Data, User's Manual, Bruker AXS, Karlsruhe, Germany, 2003.
28 PDF-2, *International Center for Diffraction Data*, Newton Square, USA, 1998.
29 Inorganic Crystal Structure Database (ICSD), Fachinformationszentrum Karlsruhe, Germany, Version 2012-1.
30 Jana 2006, Version 01/07/2011, V. Petricek, M. Dusek, L. Palatinus, Institute of Physics, Academy of science of the Czech Republic, Praha.
31 E. Keller and V. Krämer, *Z. Naturforsch.* 2005, **60b**, 1255–1263.
32 P.W. Stephens, *J. Appl. Cryst.* 1999, **32**, 291–289.
33 R.D. Shannon, *Acta Cryst.* 1976, **A32**, 751–767.
34 M. Batuk, D. Batuk, A.M. Abakumov, and J. Hadermann, *J. Solid State Chem.* 2014, **215**, 245–252.
35 D.O. Charkin, D.N. Lebedev, and S.M. Kazakov, *J. Alloys Compd.* 2012, **536**, 155–160.
36 D.O. Charkin, *Russ. J. Inorg. Chem. Suppl.* 2008, **53**, 1977–1996.
37 D.O. Charkin and X.N. Zolotova, *Crystallogr. Rev.* 2007, **13**, 201–245.
38 H. Jiang, Y.L. Sun, Z.A. Xu, and G.H. Cao, *Chin. Phys. B* 2013, **22**, 087410.
39 D.O. Charkin, S.M. Kazakov, and D.N. Lebedev, *Russ. J. Inorg. Chem.* 2010, **55**, 1248–1256.
40 A. Aliev, J. Olchowka, M. Colmont, E. Capoen, C. Wickleder, and O. Mentré, *Inorg. Chem.* 2013, **52**, 8427–8435.
41 A.T. Nientiedt, W. Jeitschko, P.G. Pollmeier, and M. Brylak, *Z. Naturforsch.* 1997, **52b**, 560–564.
42 M. Eul, D. Johrendt, and R. Pöttgen, *Z. Naturforsch.* 2009, **64b**, 1353–1359.
43 S. Katrych, K. Rogacki, A. Pisoni, S. Bosma, S. Weyeneth, R. Gaal, N.D. Zhigadlo, J. Karpinski, and L. Forr, *Phys. Rev. B* 2013, **87**, 180508.
44 M. Batuk, D. Batuk, A.A. Tsirlin, D.S. Filimonov, D.V. Sheptyakov, M. Frontzek, J. Hadermann, and A.M. Abakumov, *Chem. Mater.*, 2015, **27**, 2946–2956.

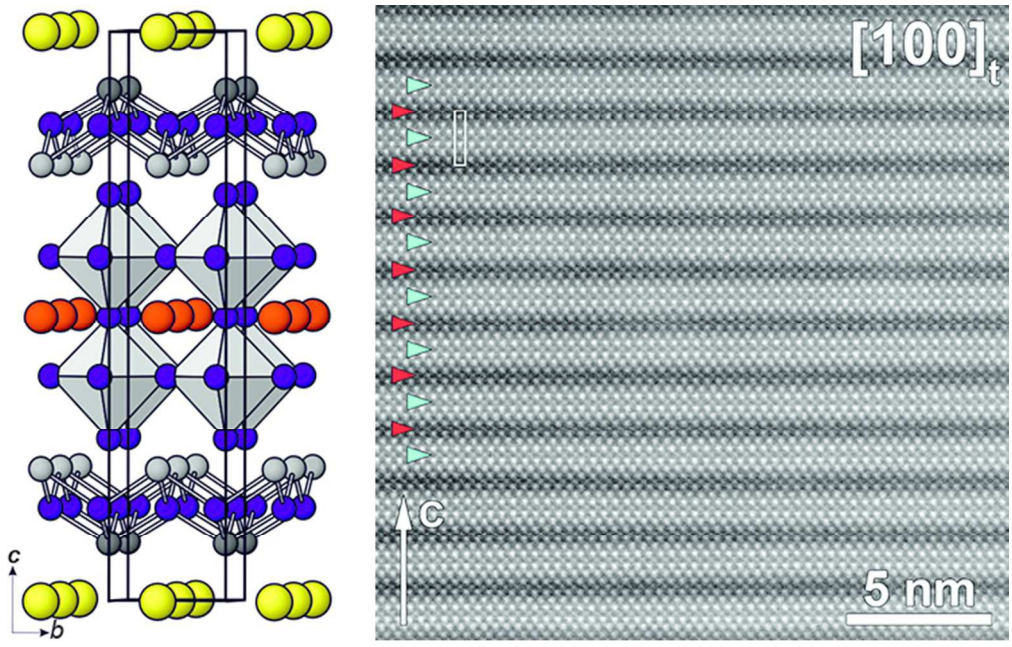

62x39mm (300 x 300 DPI)